

# Theoretic optimisation of microfluidic and magnetic self-assembly of carbon nanotubes

Joon S. Shim

Department of Convergence Electronics Engineering, Kwangwoon University, Seoul, Republic of Korea

E-mail: shim@kw.ac.kr

Published in Micro & Nano Letters; Received on 5th February 2014; Revised on 12th June 2014; Accepted on 7th July 2014

In this reported work, a magnetic and fluidic analysis has been performed to theoretically analyse the self-assembly mechanism of carbon nanotubes (CNTs) and to characterise the assembling environments for the high-density integration of individual CNTs. In previous work by the present author, the residual iron (Fe) catalyst at one end of a CNT was magnetically captured and the captured CNT was aligned along the flow direction by fluid drag force, leading to precise individual integration of CNTs between electrodes. To advance the previous work and technique, theoretic characterisations were executed to optimise the assembling conditions which increased the number of attached CNTs with a high density of integration. For calculating the fluidic force applied to the individual CNT, the slender-body theory was adopted by modelling the CNT as a slender object. Moreover, magnetic simulation was performed to calculate the magnetic force applied to the residual Fe catalyst at one end of the CNT. These simulation results were combined and used to determine the critical height where the fluidic force was equal to the magnetic force. On the basis of these analyses, the array of CNT-assembled electrodes was implemented with a 2 m interval, whereas only a single CNT-assembled electrode was achieved in the previous work. A result of the present work, enables dense integration of the CNT circuit as a highly functional nanodevice.

**1. Introduction:** In the past decades, there has been intense interest in various types of nanomaterials such as nanowires, nanotubes and nanoparticles [1]. These nanomaterials have shown superior functionalities over preexisting materials, providing breakthrough solutions for current technical limitations [2–4]. However, the assembly of these nanomaterials with integrated circuits has been a challenging issue, blocking the realisation of practical devices to fully explore the excellent properties of the nanomaterials [5–7]. As a result, there is great demand to develop the assembly technique for these nanomaterials. Furthermore, to achieve large-scale integration of nanomaterials with complex electronic circuits, the assembly mechanism should be systematically explored by theoretical simulation and experimental demonstration.

Among the various nanomaterials, carbon nanotubes (CNTs) have been extensively researched because of their excellent electrical properties [8, 9], mechanical robustness [10, 11] and chemical sensitivity [12, 13]. In our previous work, an individual CNT was precisely assembled between electrodes using a unique location of iron (Fe) catalyst at one end of the CNT [14, 15]. For the assembly of the CNT, the ferromagnetic Fe catalyst was magnetically captured in a nickel (Ni) pattern on the electrode, and the captured CNT was aligned with the flow direction by fluid drag force. In this Letter, the assembly procedure was theoretically analysed for various fluidic and magnetic conditions to optimise the CNT's assembly environments. In addition, for experimental demonstration, the theoretically optimised conditions were applied to assemble the CNTs in an array of electrodes with 2  $\mu\text{m}$  spacing, realising a densely integrated CNT circuit.

There are many reports on the theoretic analysis of CNTs [16–20]. The dynamics of a CNT in a flow could be theoretically analysed by simulation tools of molecular dynamics [16, 17] and flexible fibre dynamics [18–20]. Since the modelled CNT in this present work had a high length-to-diameter ratio of 150 (3  $\mu\text{m}$  to 20 nm), the number of calculations for the modelled CNT was too large for molecular dynamic simulation. Moreover, combinational forces of magnetic attraction and the fluid drag force should be calculated to characterise the assembly environments for our developed technique. Considering these analysis conditions, the CNT was modelled as a flexible fibre, which enabled the

theoretical analysis of the CNT's dynamics in a simple shear flow utilising continuum mechanics. For exploring the fluidic analysis, slender body theory in a simple shear flow was utilised to calculate the fluid drag force applied to the CNT [21, 22]. Moreover, magnetic and fluidic simulations by the finite element method (FEM) were carried out for a numerical analysis of the assembly mechanism. The results from these theoretical characterisations were compared with our previous experimental data, showing exact consistency for the magnetic and fluidic effects on the CNT assembly.

**2. Theoretical characterisation of CNT self-assembly:** In our previous Letter, an individual CNT was precisely located with the designed direction by the combined forces of magnetic capturing and fluidic alignment. The metal catalyst, which was a byproduct of the synthesis process of the CNT, played a key role in our assembly process. During the synthesis of the CNT, metal nanoparticles such as Fe, Ni and cobalt (Co) were utilised as a catalyst, where the CNT was grown by chemical vapour deposition (CVD) process. Thus, the metal catalyst as a seeding site of the CNT synthesis was left at one end of the CNT after the growth process. Utilising this confined position of the metal catalyst, the magnetic force was applied to grab the CNT's end and the CNT was aligned to the flow direction by the fluid drag force.

To implement a functional device with CNTs, Ni was patterned on an electrode, which induced a magnetic force under an external magnetic field. A bundle of CNTs was dispersed in the solution and flowed through the microchannel attached to the electrode-patterned substrate. When a CNT flowed over the Ni patterned electrode, the magnetic force by the Ni pattern held one end of the CNT. Finally, the fluid drag force of the flowing solution aligned the magnetically captured CNT to form a bridge between two electrodes.

**2.1. Simulation model:** To simulate the assembling force applied to the CNT, the self-assembly process was simply modelled based on the experimental data. Fig. 1 shows the schematic model of the CNT flowing in the solution. Besides, the dimensions of the modelled CNT were determined according to the average size of the experimented CNT, which was grown on the Fe catalyst by

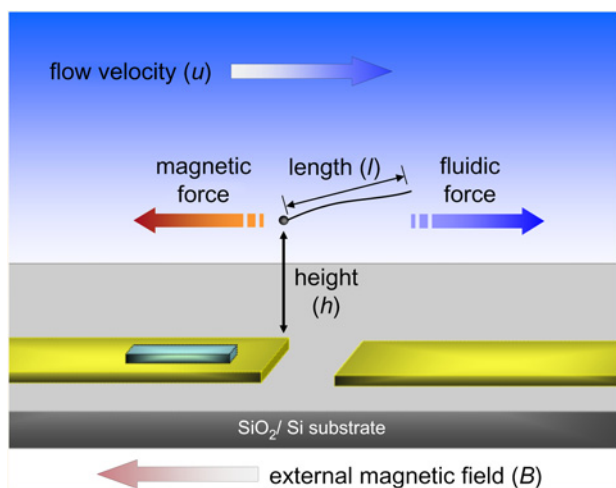


**Figure 1** Theoretical model for the magnetic and fluidic analysis of CNT assembly

To simplify the analysis, the CNT was modelled to have 3  $\mu\text{m}$  length and 50 nm diameter of the catalyst, which were the average values for the experimental CNTs

the CVD process [23]. The scanning electron microscopy (SEM) images of the CNT show that the average dimensions of the CNTs were 20 nm in diameter and 3  $\mu\text{m}$  in length. The residual Fe catalyst at one end of the CNT had a spherical shape with a diameter of 50 nm. Based on these dimensions from the experimental data, the individual CNT was simplified to have dimensions of 3  $\mu\text{m}$  length and 20 nm diameter with the 50 nm diameter catalyst at one end. In addition, the single-domain effect of a ferromagnetic material was disregarded, since the average size of the Fe catalyst was much bigger than the single-domain realm [24].

**2.2. Fluidic analysis:** To calculate the fluidic force applied to the CNT in the flow, the CNT was regarded as a slender body like a thread in the flowing solution. Based on this modelling, the fluid drag force on the surface of the CNTs was calculated by slender body theory [21, 22]. The slender body theory can be applied when the length ( $l$ ) of the body is much bigger than the radius ( $r$ ) of the body. Since the CNT model based on the experimental measurements has a very large aspect ratio ( $l/r = 3 \mu\text{m}/0.01 \mu\text{m} = 300$ ), the error term is very small, resulting in a reliable calculation of the fluidic force on the CNT by the slender body theory.

When the body's motion is governed by the Stoke's equation, and the aspect ratio ( $l/r$ ) goes to infinity, a Stokes flow does not exist around a cylindrical body. Under this condition, the slender body theory for describing the drag force ( $F$ ) applied on a CNT parallel to the axis of the flow can be derived by the following equation

$$F \simeq \frac{2\pi\mu lu}{\ln(l/r)} \quad (1)$$

where  $\mu$  is the viscosity of the solution,  $u$  the flow velocity,  $l$  the length of the CNT and  $r$  is the radius of the CNT. The simplified equation of the slender

body theory indicates that the fluidic force is linearly proportional to the flow velocity, since the CNT dimensions and the viscosity of the solution are fixed.

To calculate the fluid drag force, the flow velocity ( $u$ ) according to the height is simulated by CFD-ACS + (ESI-CFD, Inc.). During the self-assembly process in our experiments, the CNT solution was flowed through a PDMS (polydimethylsiloxane) microchannel attached to the Ni-patterned electrodes. Since the experimented

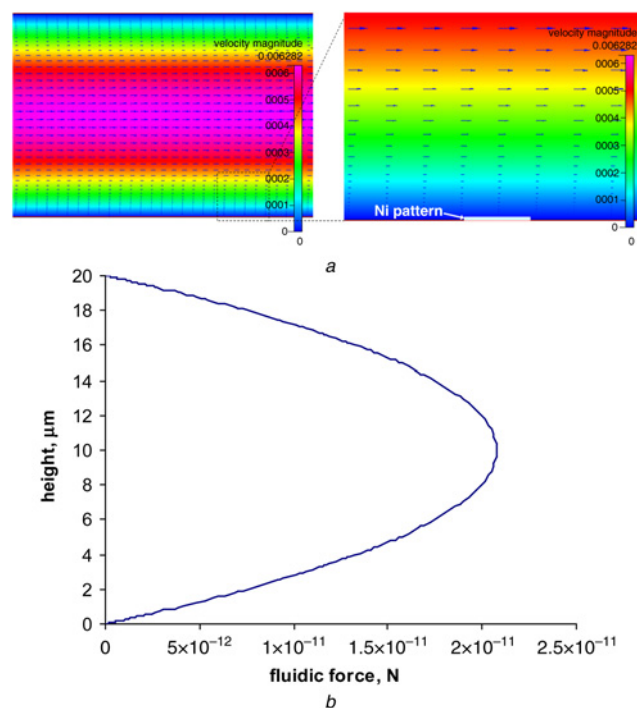


**Figure 2** Fluidic simulation by CFD-ACE+

*a* Cut view of simulated flow velocity in a microchannel (20  $\mu\text{m}$  thickness and 2 mm width)

*b* Fluidic force to the CNT according to the height at a flow velocity of 4.2 mm/s. The slender-body theory was applied to simulate the flow velocity inside a microchannel

microchannel was 20  $\mu\text{m}$  high and 2 mm wide, the microfluidic simulation was performed for a microchannel with the same dimensions, and the result is plotted in Fig. 2*a*. With this designed microchannel, various flow velocities were simulated to characterise the fluid drag force applied to the CNT. After calculating the profile of the flow velocity inside the microchannel, the velocity profile was utilised to calculate the fluidic force with (1). By applying 3  $\mu\text{m}$  length and 20 nm diameter, as the dimensions of the simplified model of the CNT, the fluidic force acting on the CNT at a flow velocity of 4.2 mm/s was simulated according to the height of the microchannel, as plotted in Fig. 2*b*. Owing to the non-slip boundary effect near the microchannel boundary, the flow velocity has a parabolic profile with respect to the height of the microchannel, resulting in a faster flow at the microchannel centre. Since the flow velocity approaches zero at the microchannel boundary, the fluid drag force to the CNT is very low at the bottom of the microchannel. As a result, the CNTs near the Ni pattern have a much higher chance of assembly than the CNTs at the centre of the microchannel.

**2.3. Magnetic analysis:** Although the fluidic force dragged the CNT, the Fe catalyst at one end of the CNT was magnetically attracted by the Ni pattern. Under the external magnetic field, a magnetic gradient is generated around the Ni pattern, which induces the localised magnetic force at the edge of the Ni pattern. Since the residual Fe catalyst is a ferromagnetic material and located at one side of the CNT after its synthesis process, the Fe catalyst of the CNT is magnetically attracted by the Ni pattern and positioned at the edge of the Ni pattern, which is designed to be a target location of the CNT assembly. To calculate this magnetic force applied to the Fe catalyst of the CNT, the induced magnetic force at the Ni pattern under the external magnetic field was simulated by the following equation

$$F = m \cdot \nabla B \quad (2)$$

where  $m$  is the magnetic momentum of the Fe catalyst and  $B$  is the magnetic field induced by the Ni pattern [25]. Owing to the spherical shape of the Fe catalyst, the magnetic momentum of the Fe catalyst is constant for all directions, so the magnetic force is linearly proportional to the gradient of the magnetic field.

As the SEM images of the experimented CNT indicated that the diameter of the catalyst was 50 nm, the magnetic momentum of the 50 nm Fe nanoparticle ( $m \sim 6 \times 10^{-17} \text{ A m}^2$ ) was used [26]. The magnetic force between the Ni pattern and the Fe catalyst was simulated by MagNet (MagNet, Infolytica, Inc.) and the result was analysed with respect to the position of the CNT in the microchannel. To characterise the effect of the magnetic force, Ni structures with different dimensions (0.2, 0.5, 1 and 2  $\mu\text{m}$  in length) were simulated, while the width and thickness were fixed to 0.2 and 0.1  $\mu\text{m}$ , respectively. Moreover, a uniform external magnetic field of 0.7 T was given to the longitudinal direction of the Ni pattern, which was a sufficiently strong magnetic field in the laboratory environment.

Fig. 3a shows the simulation result for the magnetic field about the 2  $\mu\text{m}$  long Ni pattern under an external magnetic field of 0.7 T. The contour lines, which represent lines of equal magnetic fields, are very dense at the edge of the Ni pattern. This indicates that the localised and high gradient of the magnetic field is generated at the edge of the Ni pattern. With this simulation result of the magnetic field, the magnetic force is calculated by (2) and plotted in Fig. 3b, which displays the magnetic force applied to the Fe catalyst along the longitudinal direction of the Ni pattern. Owing to the ferromagnetic property of Ni, the magnetic field is largely changed around the Ni pattern. So, the strong gradient of

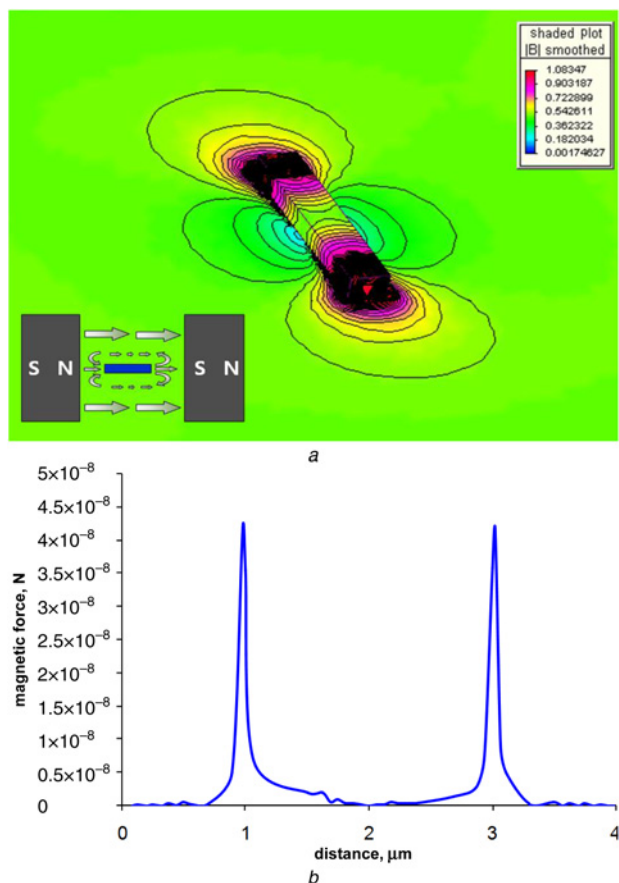


**Figure 3** Magnetic simulation result under an external magnetic field of 0.7 T

a Contour lines representing lines of equal magnetic field around the Ni pattern  
b Induced magnetic force about the 2  $\mu\text{m}$  long Ni pattern  
The result displays the high magnetic force generated at the edge of the Ni pattern

the magnetic field is generated at the edge of the Ni pattern. Since the magnetic force is dependent on the gradient of the magnetic field in (2), the magnetic force is localised at the edge of the Ni pattern. As a result, the Fe catalyst of the CNT is selectively assembled at the end of the Ni pattern.

When the CNT is flowed through the microchannel under the external magnetic field, the magnetic force applied to the Fe catalyst attracts the CNT, and the fluidic force drags the CNT to the flow direction. Thus, the magnetic and fluidic forces are competitively applied to the CNT in an opposite direction, determining whether the CNT is assembled or not. To assemble the CNT at the edge of the Ni pattern, the magnetic force attracting one end of the CNT should be larger than the fluidic force dragging the CNT. When the CNT approached the Ni pattern, the magnetic force increased because of the shorter distance between the CNT's catalyst and the Ni pattern. On the other hand, as the CNT's position is close to the centre of the microchannel height, the flow velocity becomes higher, increasing the fluid drag force on the CNT.

**2.4. Critical height:** To numerically analyse the self-assembly mechanism of the CNT, the magnetic force and fluidic force were characterised according to the height of the CNT's position from the Ni pattern. As the fluidic force and the magnetic force were applied to the CNT in the opposite direction, the critical height was determined, where the magnetic force was equal to the fluidic force.

Fig. 4a shows the process of calculating the critical height. The magnetic force was sharply decreased as the distance of the CNT from the Ni pattern was increased. In contrast, the fluidic force was increased as the height of the CNT from the Ni pattern was increased, because the CNT was close to the centre of the

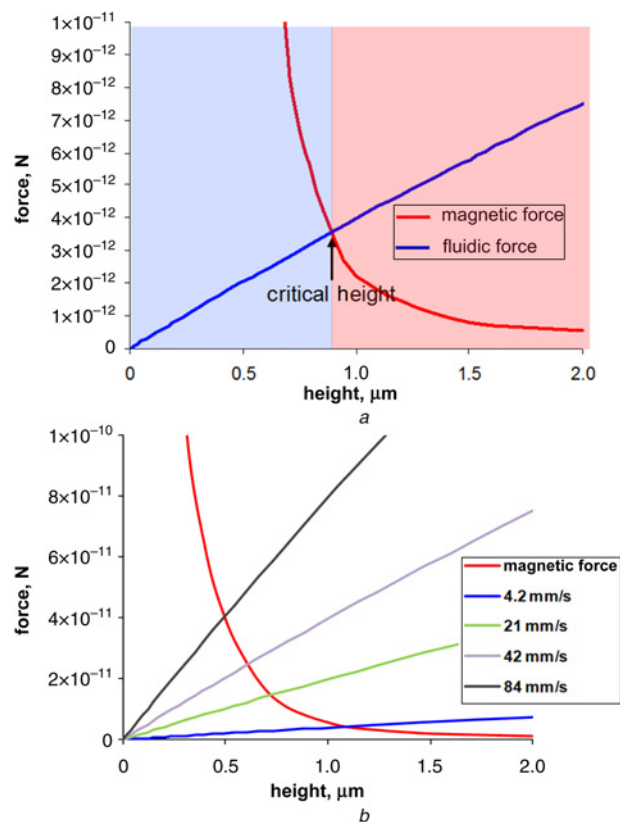


**Figure 4** Simulated magnetic force and the fluid drag force against height above the Ni pattern

Critical height for capturing CNTs can be determined where the magnetic force is equal to the fluid drag force

a Magnetic force  
b Fluid drag force

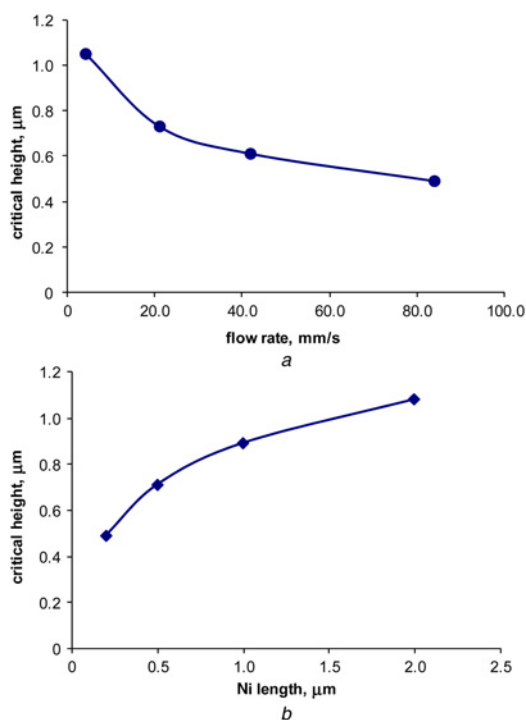


**Figure 5** Numerical simulation results of critical height according to flow velocity and size of Ni pattern  
*a* Flow velocity  
*b* Size of Ni pattern

microchannel. Owing to the conflicting tendency of each force, the critical height could be defined as a height where the graph of the magnetic force crosses with the one of the fluidic forces, leading to a position of force equilibrium for the CNT. The magnetic force is dominant below the critical height (the left side of Fig. 4a), whereas the fluidic force is dominant over the critical height (the right side of Fig. 4a). To assemble the CNT at the Ni pattern, the CNT should be in the region where the magnetic force is dominant.

By changing the microfluidic and magnetic conditions, the critical height for the CNT assembly could be modulated. To optimise the CNT assembly conditions, the numerical analyses were executed for characterising the effects of control variables such as flow velocity and the dimensions of the Ni pattern. In the case of flow velocity, the fluid drag force for the various flow velocities was simulated, and the results are displayed with the magnetic force for the Ni pattern with 2 μm length as in Fig. 4b. As the flow velocity decreased, the fluidic force is more slowly increased according to the CNT's height. Thus, at the lower flow velocity, the fluidic force crossed with the magnetic force at the higher position, increasing the critical height. On the basis of this analysis, the critical heights were numerically attained for various flow velocities of 4.2, 21, 42 and 84 mm/s as plotted in Fig. 5a. In the same way, the magnetic force was simulated for various lengths of the Ni pattern. Since the longer Ni pattern generated higher magnetic gradients, the magnetic force was increased as the length of the Ni pattern increased. As a result, the critical height was increased with the Ni pattern length as shown in Fig. 5b.

**3. Experimental details:** For the fabrication of electrodes, e-beam lithography was executed on an SiO<sub>2</sub>/Si substrate with a conventional lift-off process. After patterning the Au/Ti electrodes, Ni patterns of width 200 nm and of length 1 μm were patterned on the Au/Ti electrodes by the multilayer technique of e-beam lithography. The Ni patterns and electrodes were designed to provide 1 μm contact length to the assembled CNT.

The experimented CNTs were purchased from FirstNano (FirstNano Inc., USA), which were vertical-array type multi-walled nanotubes (MWNTs) grown on an SiO<sub>2</sub>/Si substrate. To individually assemble the CNT on the electrode, the vertical arrays of CNTs were dispersed in 1 wt% Tween-20 solution mixed in deionised (DI) water. For dispersing the CNTs in the solution, the CNT-containing solution was sonicated in an ultrasonic bath (Branson Ultrasonic Corp., USA) for 30 min.

To flow the CNT solution in a microchannel, soft lithography with poly(dimethylsiloxane) (PDMS) was used with a photoresist mould fabricated with AZ4620 (AZ Electronic Materials Corp., USA). The fabricated microchannel has cross-sectional dimensions of 20 μm width and 2 mm height. After aligning the Ni patterned electrodes at the centre of the microchannel, the PDMS microchannel was attached on the fabricated SiO<sub>2</sub>/Si substrate. The PDMS microchannel-attached device was placed on a set of permanent magnets which provides 0.7 T of magnetic field to the Ni patterns at the device. Then, the CNT solution flowed through the microchannel with a flow velocity of 4.2 mm/s which was controlled by a syringe pump (Harvard Apparatus Inc., USA). As the PDMS microchannel and the SiO<sub>2</sub>/Si substrate were not processed by oxygen plasma treatment, the microchannel could be detached after the CNT assembly process. To reduce the contact resistance between the CNT and the electrode, an annealing process was performed at 350°C for 5 min under a flow of nitrogen (N<sub>2</sub>) by rapid thermal process (RTP, AG Associates Inc., USA).

**4. Results and discussion:** The results from the theoretic analyses were compared with the experimental results reported in our previous work [14]. To experimentally characterise the effects of the fluidic and magnetic forces, the number of the assembled CNTs was counted in various environments. As the critical height increased, the number of the CNTs that flowed below the critical height was also increased. Thus, in accordance with the fluidic simulation, the experimentally counted number of the assembled CNTs was increased as the flow velocity decreased. Similarly, the number of the assembled CNTs was increased as the length of the Ni pattern increased. In addition, the changes of the experimental results for the number of assembled CNTs had a tendency similar to the simulation results, which demonstrates a good agreement of the theoretical analyses with the experimental results.

In addition, the experimental results showed that a higher flow velocity results in a better alignment of the assembled CNTs to the flow direction. As the fluid drag force to the CNT was increased with the flow velocity, the CNTs were better aligned along the flow direction at higher flow velocity. Therefore, when the flow velocity was reduced, more CNTs were captured by the magnetic force, but the alignment along the flow direction became poor. On the other hand, higher flow velocities resulted in a reduced number of CNTs assembled on the Ni contact, but the assembled CNTs were more precisely aligned in a specified direction. Considering the loss of CNTs at higher flow velocity, 10 μl volume of the CNT solution was flowed over the prepared electrode. The optimised conditions for the CNT assembly have been established based on these theoretical and experimental analyses. To ensure the CNT assembly at each electrode and to improve the alignment of the CNTs along the flow direction, the flow velocity and the length of the Ni pattern were set to be 4.2 mm/s and 1 μm, respectively. The simulation results proved that the critical height at these conditions was 0.87 μm.

To show the feasibility of an integrated CNT-assembled circuit, a sequential array of the assembled CNTs with a high-density interval of 2 μm was achieved, as shown in Fig. 6a. The precise assembly of multiple CNTs shows the feasibility of this technique for the creation of densely assembled CNT circuitry.

To electrically characterise the assembled CNT, the current-voltage (*I-V*) curve was measured as presented in Fig. 6b. In this Letter, MWNTs were assembled between electrodes. Consistent



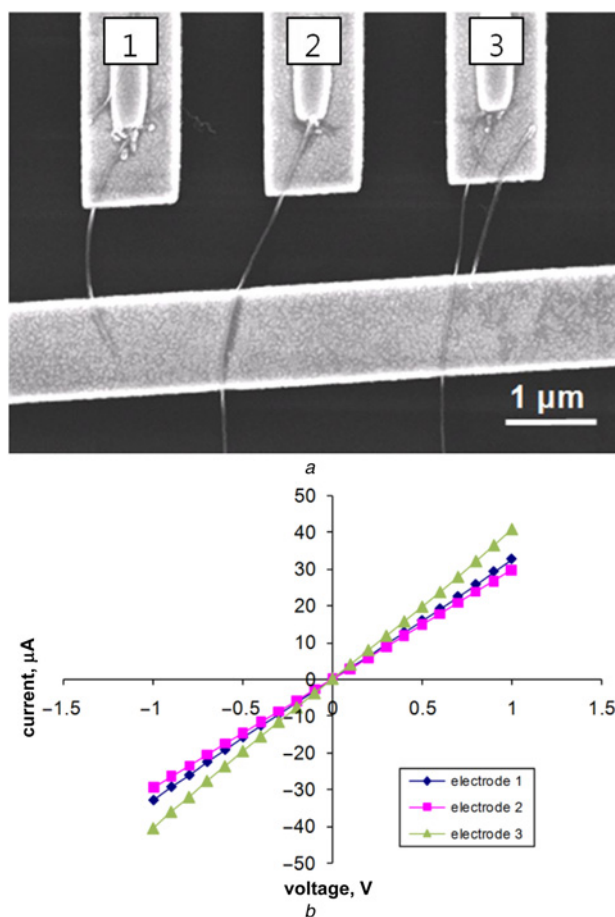


**Figure 6** SEM image of sequentially aligned MWNTs array with 2  $\mu\text{m}$  interval, and Current–voltage response from the CNT assembled electrodes  
a SEM image  
b Current–voltage response

with the previous reports in which MWNTs usually possessed metallic properties [27, 28], linear relationships between the current and the voltage were recorded for all the CNTs. This linear relationship demonstrated good ohmic contact between the Au/Ti electrodes and the assembled CNTs. The measured resistances of the assembled CNTs were 33.7, 30.5 and 24.6 k $\Omega$ , respectively. The resistance difference between electrode 1 and electrode 2 was caused by the contact length between the electrodes and the assembled CNTs [28]. Also, for electrode 3, two CNTs were assembled between the electrodes, so it was expected that the measured resistance would be half the average of the others. However, one of them has a short contact length to the electrodes, resulting in a large resistance although two CNTs were assembled between the electrodes.

In this Letter, a theoretical optimisation and an experimental demonstration have been performed to analyse the fluidic and magnetic conditions necessary for the self-assembly of CNTs. Using the average sizes of the CNTs in the experiments, the CNT was theoretically modelled to simulate the magnetic force and the fluidic force. On the basis of the simulated results, the critical height for capturing CNTs was calculated. The theoretical results were well matched with the experimental results, showing that a successful analysis was achieved in this work.

**5. Conclusion:** The fluidic and magnetic self-assembly mechanism of a CNT has been theoretically analysed and experimentally demonstrated for optimising the assembly conditions. Since the magnetic attraction and the fluid drag force were applied to the CNT in the opposite direction, the critical height where the

magnetic force equalled the fluidic force was calculated to explore the effects of various assembly conditions. Based on the theoretical characterisations from the fluidic and magnetic simulations, the assembly conditions were established to be 4.2 mm/s of flow velocity and 1  $\mu\text{m}$  of Ni length. Utilising these theoretic analyses, the individual CNTs have been successfully assembled in a densely integrated electrode array in this Letter. The theoretic analysis for the self-assembly of an individual CNT can be widely applied to implement a highly integrated nanodevice with various nanomaterials.

**6. Acknowledgment:** The authors acknowledge the support of this work by the Kwangwoon Research Grant of 2013.

## 7 References

- [1] Klabunde K.J.: 'Nanoscale materials in chemistry' (John Wiley & Sons, Inc., New York, 2001)
- [2] Wanga J.: 'Analyst', 2005, **130**, pp. 421–426
- [3] Vikesland P.J., Wigginton K.R.: 'Nanomaterial enabled biosensors for pathogen monitoring', *Environ. Sci. Technol.*, 2010, **44**, pp. 3656–3669
- [4] Hoenlein W., Duesberg G.S., Graham A.P., *ET AL.*: 'Nanoelectronics beyond silicon', *Microelectron. Eng.*, 2006, **83**, pp. 619–623
- [5] McEuen P.L., Fuhrer M.S., Park H.: 'Single-walled carbon nanotube electronics', *IEEE Trans. Nanotechnol.*, 2002, **1**, pp. 78–84
- [6] Dai L., Patil A., Gong X., *ET AL.*: 'Aligned nanotubes', *Chem. Phys. Chem.*, 2003, **4**, pp. 1150–1169
- [7] Yan Y., Chan-Park M.B., Zhang Q.: 'Advances in carbon-nanotube assembly', *Small*, 2007, **3**, pp. 24–42
- [8] Collins P.G., Bradley K., Ishigami M., Zettl A.: 'Extreme oxygen sensitivity of electronic properties of carbon nanotubes', *Science*, 2000, **287**, pp. 1801–1804
- [9] Kong J., Franklin N.R., Zhou C., *ET AL.*: 'Nanotube molecular wires as chemical sensors', *Science*, 2000, **287**, pp. 622–625
- [10] Yakobson B.I., Smalley R.E.: 'Fullerene nanotubes: C1 000 000 and beyond', *Am. Sci.*, 1997, **85**, pp. 324–337
- [11] Yu M., Lourie O., Dyer M.J., Moloni K., Kelly T.F., Ruoff R.S.: 'Strength and breaking mechanism of multiwalled carbon nanotubes under tensile load', *Science*, 2000, **287**, pp. 637–640
- [12] White C.T., Todorov T.N.: 'Carbon nanotubes as long ballistic conductors', *Nature*, 1998, **393**, pp. 240–241
- [13] Bachtold A., Hadley P., Nakanishi T., Dekker C.: 'Logic circuits with carbon nanotube transistors', *Science*, 2001, **294**, pp. 1317–1320
- [14] Shim J.S., Yun Y.H., Rust M.J., *ET AL.*: 'The precise self-assembly of individual carbon nanotubes using magnetic capturing and fluidic alignment', *Nanotechnology*, 2009, **20**, p. 325607
- [15] Shim J.S., Yun Y.H., Cho W., Shanov V., Schulz M.J., Ahn C.H.: 'Self-aligned nanogaps on multilayer electrodes for fluidic and magnetic assembly of carbon nanotubes', *Langmuir*, 2010, **26**, pp. 11642–11647
- [16] Tang W., Advani S.G.: 'Drag on a nanotube in uniform liquid argon flow', *J. Chem. Phys.*, 2006, **125**, p. 174706
- [17] Walther J.H., Werder T., Jaffe R.L., Koumoutsakos P.: 'Hydrodynamic properties of carbon nanotubes', *Phys. Rev. E*, 2004, **69**, p. 062201
- [18] Dimaki M., Bøggild P.: 'Dielectrophoresis of carbon nanotubes using microelectrodes: a numerical study', *Nanotechnology*, 2004, **15**, pp. 1095–1102
- [19] Tang W., Advani S.G.: 'Dynamic simulation of carbon nanotubes in simple shear flow', *CMEs*, 2008, **25**, (3), pp. 149–164
- [20] Tang W., Advani S.G.: 'Non-equilibrium molecular dynamics simulation of water flow around a carbon nanotube', *CMEs: Comput. Model. Eng. Sci.*, 2005, **8**, pp. 165–176
- [21] Cox R.G.: 'The motion of long slender bodies in a viscous fluid. Part 1. General theory', *J. Fluid Mech.*, 1970, **44**, p. 791
- [22] Batchelor G.K.: 'Slender-body theory for particles of arbitrary cross-section in Stokes flow', *J. Fluid Mech.*, 1970, **44**, p. 419
- [23] Yun Y., Shanov Y., Tu Y., Subramaniam S., Schulz M.J.: 'Growth mechanism of long aligned multiwall carbon nanotube arrays by water-assisted chemical vapor deposition', *J. Phys. Chem. B*, 2006, **110**, pp. 23920–23925
- [24] Gupta A.K., Gupta M.: 'Synthesis and surface engineering of iron oxide nanoparticles for biomedical applications', *Biomaterials*, 2005, **26**, pp. 3995–4021

- [25] Pankhurst Q.A., Connolly J., Jones S.K., Dobson J.: 'Applications of magnetic nanoparticles in biomedicine', *J. Phys. D, Appl. Phys.*, 2003, **36**, pp. R167–R181
- [26] Kim H.K., Hong S.H., Hwang S.W., *ET AL.*: 'Magnetic capture of a single magnetic nanoparticle using nanoelectromagnets', *J. Appl. Phys.*, 2005, **98**, pp. 1–4
- [27] Wakaya F., Katayama K., Gamo K.: 'Contact resistance of multiwall carbon nanotubes', *Microelectron. Eng.*, 2003, **67/68**, pp. 853–857
- [28] Lan C., Srisungsitthisunti P., Amama P.B., Fisher T.S., Xu X.F., Reifenberger R.G.: 'Measurement of metal/carbon nanotube contact resistance by adjusting contact length using laser ablation', *Nanotechnology*, 2008, **19**, p. 125703